

## Deep Blue Fluorescent Host Materials Based on a Novel Spiro[benzo[*c*]fluorene-7,9'-fluorene] Core Structure with Side Aromatic Wings

In-Ho Lee, Jeong-A Seo, and Myoung-Seon Gong\*

Department of Nanobiomedical Science and WCU Research Center of Nanobiomedical Science, Dankook University, Chungnam 330-714, Korea. \*E-mail: msgong@dankook.ac.kr  
Received March 24, 2012, Accepted April 9, 2012

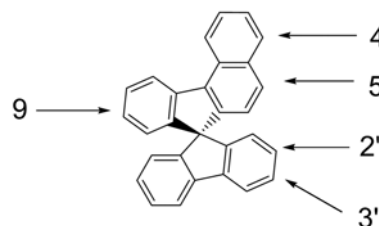
Deep blue fluorescent host materials based on a novel spiro[benzo[*c*]fluorene-7,9'-fluorene] core structure with side aromatic wings in the 5- and 9-positions, namely, 5,9-di(naphthalen-2-yl)spiro[benzo[*c*]fluorene-7,9'-fluorene] (**DN-SBFF**), 5,9-bis(4-*t*-butylphenyl)spiro[benzo[*c*]fluorene-7,9'-fluorene] (**BP-SBFF**), and 5,9-bis(4-fluorophenyl)spiro[benzo[*c*]fluorene-7,9'-fluorene] (**FP-SBFF**), were designed and successfully prepared using the Suzuki reaction. The physical properties of these materials and their EL characteristics as blue host materials doped with *N,N,N',N'*-tetraphenylspiro[benzo[*c*]fluorene-7,9'-fluorene]-5,9-diamine (**TPA-SBFF**) were investigated. The device used comprised ITO/*N,N'*-diphenyl-*N,N'*-bis[4-(phenyl-*m*-tolyl-amino)phenyl]-biphenyl-4,4'-diamine (DNTPD)/*N,N'*-di(1-naphthyl)-*N,N'*-diphenylbenzidine (NPB)/(**FP-SBFF**):dopant x%/tris(8-hydroxyquinoline)aluminum (Alq<sub>3</sub>)/LiF. The device obtained using **FP-SBFF** doped with **TPA-SBFF** showed high color purity (0.13, 0.18) and an efficiency of 6.61 cd/A at 7 V.

**Key Words** : Blue OLED, Blue host, Spiro[benzo[*c*]fluorene-7,9'-fluorene], Color purity

### Introduction

Organic light-emitting diodes (OLEDs) are used widely as emissive devices in lighting and flat panel displays because of their low driving voltages, low power consumptions, high color gamut, high contrasts, and rapid responses.<sup>1-4</sup> The three basic color components red, green, and blue are needed to obtain a full color display. Although red and green emitters for organic EL devices are readily available, efficient and stable organic blue emitters are rare, and as a result, the development of high-performance blue-emitting organic devices is a subject of considerable interest.<sup>5-7</sup> Furthermore, despite the considerable advances made in the OLED field, it is difficult to find appropriate blue emitting materials because of their low solution and low solid-state photoluminescence (PL) quantum yields.<sup>8</sup>

Spiro-type derivatives containing fluorene or benzofluorene have received a great deal of attention as fluorescent materials for OLEDs, because they preserve the inherent characteristics of spiro compounds, such as, morphological stability, a high glass transition temperature, and amorphous property. They also provide the ability to attach different substituents on the spiro[benzo[*c*]fluorene-7,9'-fluorene] (**SBFF**) because of their asymmetrical spiro core structures composed of naphthalene and phenylene rings. Therefore conjugation-controlled OLEDs host and dopant materials are obtainable as shown in Scheme 1. Many studies have addressed the use of **SBFFs** as organic electroluminescent host materials, and it has been established that the performances of OLEDs (*i.e.*, color purity and luminescence efficiency) based on **SBFF** are determined by the positions of substituents, aryl moiety type and conjugation chain length.<sup>9-17</sup>



**Scheme 1.** Positions of substituents in spiro[benzo[*c*]fluorene-7,9'-fluorene].

In this work, a novel **SBFF** core structure with aromatic side wings was developed as a highly fluorescent deep blue host material with good thermal/morphological stability and the physical properties. Three new deep blue host materials, namely 5,9-di(naphthalen-2-yl)spiro[benzo[*c*]fluorene-7,9'-fluorene] (**DN-SBFF**), 5,9-bis(4-*t*-butylphenyl)spiro[benzo[*c*]fluorene-7,9'-fluorene] (**BP-SBFF**), and 5,9-bis(4-fluorophenyl)spiro[benzo[*c*]fluorene-7,9'-fluorene] (**FP-SBFF**) were prepared and characterized by <sup>1</sup>H NMR, <sup>13</sup>C NMR, FT-IR, mass spectroscopy, thermal analysis, UV-vis, and PL spectroscopy. The EL properties of multilayered OLEDs fabricated by using three host materials and *N,N,N',N'*-tetraphenylspiro[benzo[*c*]fluorene-7,9'-fluorene]-5,9-diamine (**TPA-SBFF**) as dopant were evaluated.

### Experimental

**Materials and Measurements.** Tetrakis(triphenylphosphine)palladium(0), 4-fluorophenylboronic acid, 4-*tert*-butylphenylboronic acid, and naphthalene-2-boronic acid (Aldrich Chem. Co.) were used without further purification. 5,9-Dibromospiro[benzo[*c*]fluorene-7,9'-fluorene] (5,9-di-

bromo-SBFF) and *N,N,N',N'*-tetraphenylspiro[benzo[*c*]fluorene-7,9'-fluorene]-5,9-diamine (TPA-SBFF) were prepared as previously described.<sup>13,18,19</sup>

Photoluminescence (PL) spectra were recorded on a fluorescence spectrophotometer (Jasco FP-6500) and UV-vis spectra were obtained by using a UV-vis spectrophotometer (Shimadzu, UV-1601PC). Energy levels were measured by using a low-energy photo-electron spectrometer (Riken-Keiki AC-2). The FT-IR spectra were obtained by using a Thermo Fisher Nicolet 850 spectrophotometer and elemental analyses were performed by using a CE Instrument EA1110. The DSC measurements were performed on a SHIMADZU DSC-60 differential scanning calorimeter under nitrogen at a heating rate of 10 °C/min. TGA measurements were performed on a SHIMADZU TGA-50 Thermo gravimetric analyzer at a heating rate of 5 °C/min, and finally, low and high resolution mass spectra were recorded by using a JEOL JMS-AX505WA spectrometer in FAB mode.

**Representative Preparation of 5,9-Diaryl-spiro[benzo[*c*]fluorene-7,9'-fluorene].** A solution of 5,9-dibromo-SBFF (5.00 g, 9.53 mmol), naphthalene-2-boronic acid (3.93 g, 22.88 mmol), tetrakis(triphenylphosphine) palladium(0) (1.1 g, 0.95 mmol) in THF (50 mL) were stirred in a two-necked flask for 30 min. To the resulting solution, was added potassium carbonate (1.31 g, 9.53 mmol) dropwise over 20 min. The resulting reaction mixture was refluxed overnight at 80 °C, and then extracted with ethylacetate and water. After evaporating off the organic layer using a rotary evaporator, the resulting powder was purified by column chromatography from *n*-hexane to give 5,9-di(naphthalen-2-yl)spiro[benzo[*c*]fluorene-7,9'-fluorene] (DN-SBFF) as a white crystalline product. The other host material, 5,9-bis(4-tert-butylphenyl)-spiro[benzo[*c*]fluorene-7,9'-fluorene] (BP-SBFF) and 5,9-bis(4-fluorophenyl)-spiro[benzo[*c*]fluorene-7,9'-fluorene] (FP-SBFF) were prepared by using similar procedures.

**DN-SBFF:** Yield 76%. mp 256.5 °C. <sup>1</sup>H NMR (500 MHz, CDCl<sub>3</sub>) δ 8.76-8.75 (d, *J* = 8.50 Hz, 1H, Ar-CH-benzene), 8.19-8.18 (d, *J* = 8.32 Hz, 1H, Ar-CH-benzene), 8.05-8.03 (d, *J* = 8.20 Hz, 1H, Ar-CH-benzene), 7.82-7.71 (m, 5H, Ar-CH-fluorene), 7.47-7.40 (m, 7H, Ar-CH-fluorene), 7.38-7.31 (m, 4H, Ar-CH-naphthalene), 7.14-7.06 (m, 10H, Ar-CH-naphthalene), 6.85-6.76 (m, 2H, Ar-CH-benzene), <sup>13</sup>C NMR (CDCl<sub>3</sub>) δ 150.2, 148.1, 147.5, 142.4, 142.3, 138.4, 133.4, 128.9, 128.7, 128.0, 127.8, 126.6, 126.0, 125.1, 124.6, 124.3, 124.2, 123.5, 120.3, 119.9, 110.3, 77.4, 77.2, 76.9, 66.5 ppm. FT-IR (KBr, cm<sup>-1</sup>) 3052, 3016 (aromatic C-H). MS (FAB) *m/z* 618.23 [(*M* + 1)<sup>+</sup>]. UV/Vis (THF): λ<sub>max</sub> (Absorption) = 364 nm, λ<sub>max</sub> (Emission) = 430 nm.

**BP-SBFF:** Yield 68%. mp 259 °C. <sup>1</sup>H NMR (500 MHz, CDCl<sub>3</sub>) δ 8.95-8.93 (d, *J* = 8.42 Hz, 1H, Ar-CH-benzene), 8.50-8.49 (d, *J* = 8.20 Hz, 1H, Ar-CH-benzene), 8.06-8.04 (d, *J* = 8.40 Hz, 1H, Ar-CH-benzene), 7.84-7.82 (d, 2H, Ar-CH-benzene), 7.74-7.72 (t, 2H, Ar-CH-naphthalene), 7.71-7.70 (q, 3H, Ar-CH-naphthalene), 7.52-7.50 (m, 4H, Ar-CH-benzene), 7.41-7.34 (m, 3H, Ar-CH-benzene), 7.10-7.07 (t, 2H, Ar-CH-benzene), 6.99-6.98 (d, 2H, Ar-CH-benzene),

6.79-6.78 (d, 2H, Ar-CH-benzene), 6.76-6.75 (d, 1H, Ar-CH-Ar), 1.32-1.29 (s, 18H, *t*-butyl-benzene), <sup>13</sup>C NMR (CDCl<sub>3</sub>) δ 149.9, 148.1, 142.3, 141.1, 140.9, 132.4, 130.3, 128.2, 128.0, 127.7, 127.4, 127.1, 126.8, 125.7, 124.3, 124.2, 123.2, 120.2, 77.4, 77.2, 76.9, 66.5 ppm. FT-IR (KBr, cm<sup>-1</sup>) 3059, 3040, 3012 (aromatic C-H). MS (FAB) *m/z* 630.33 [(*M* + 1)<sup>+</sup>]. UV/Vis (THF): λ<sub>max</sub> (Absorption) = 359 nm, λ<sub>max</sub> (Emission) = 426 nm.

**FP-SBFF:** Yield 68%. mp 259 °C. <sup>1</sup>H NMR (500 MHz, CDCl<sub>3</sub>) δ 8.95-8.93 (d, *J* = 8.42 Hz, 1H, Ar-CH-benzene), 8.52-8.50 (d, *J* = 8.20 Hz, 1H, Ar-CH-benzene), 7.94-7.92 (d, *J* = 8.450 Hz, 1H, Ar-CH-benzene), 7.87-7.85 (d, *J* = 7.65 Hz, 1H, Ar-CH-benzene), 7.75-7.68 (t, 2H, Ar-CH-naphthalene), 7.66-7.65 (d, 1H, Ar-CH-benzene), 7.52-7.50 (t, 1H, Ar-CH-naphthalene), 7.43-7.40 (m, 4H, Ar-CH-benzene), 7.28-7.25 (m, 2H, Ar-CH-benzene), 7.12-7.11 (t, 2H, Ar-CH-benzene), 7.01-7.00 (d, 4H, Ar-CH-benzene), 7.00-6.99 (d, 1H, Ar-CH-benzene), 6.95-6.94 (d, 2H, Ar-CH-Ar), 6.71-6.70 (d, 1H, Ar-CH-benzene), <sup>13</sup>C NMR (CDCl<sub>3</sub>) δ 152.0, 148.2, 147.6, 142.4, 142.1, 140.8, 136.4, 135.8, 134.2, 129.7, 128.0, 127.7, 127.4, 127.1, 126.8, 125.7, 124.3, 124.2, 123.2, 120.2, 77.5, 77.2, 76.9, 66.6 ppm. FT-IR (KBr, cm<sup>-1</sup>) 3059, 3040, 3012 (aromatic C-H). MS (FAB) *m/z* 554.18 [(*M* + 1)<sup>+</sup>]. UV/Vis (THF): λ<sub>max</sub> (Absorption) = 355 nm, λ<sub>max</sub> (Emission) = 418 nm.

**OLED Fabrication.** The basic device configuration used was indium tin oxide (ITO, 150 nm)/*N,N'*-diphenyl-*N,N'*-bis-[4-(phenyl-*m*-tolyl-amino)-phenyl]-biphenyl-4,4'-diamine

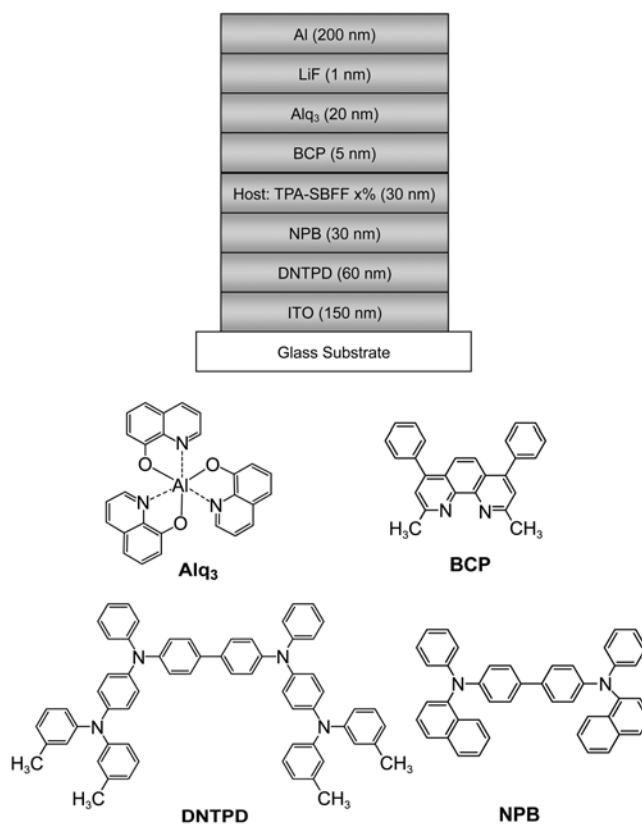


**Figure 1.** The device configuration and the chemical structure of the materials used in the devices.

(DNTPD, 60 nm)/*N,N'*-di(1-naphthyl)-*N,N'*-diphenylbenzidine ( $\alpha$ -NPB, 30 nm)/host: **TPA-SBFF** (30 nm, x%)/tris(8-hydroxyquinoline)aluminum (Alq<sub>3</sub>, 20 nm)/LiF (1 nm)/Al (200 nm) as shown in Figure 1. Organic layers were deposited sequentially onto a substrate at a rate of 1.0 Å/s by thermal evaporation from heated alumina crucibles. The doping concentrations of the dopant materials were 3, 5, 7 and 10% (wt/wt). The devices were encapsulated with a glass lid and a CaO getter after cathode deposition. Current density-voltage-luminance and electroluminescence characteristics of the blue fluorescent OLEDs were measured by using a Keithley 2400 source measurement unit and a CS 1000 spectroradiometer.

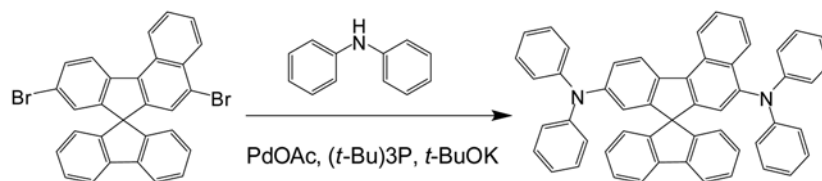
## Results and Discussion

**Synthesis and Characterization.** Dopant material **TPA-SBFF** was prepared as shown in Scheme 2, and 5,9-Dibromo-SBFF was prepared by selective bromination of **SBFF** using carbon tetrachloride and chloroform solvent as shown in Scheme 3. The host materials **DN-SBFF**, **BP-SBFF**, and **FP-SBFF** were prepared *via* the Suzuki reaction by reacting 5,9-dibromo-SBFF with naphthalen-2-ylboronic acid, 4-*tert*-butylphenylboronic acid, or 4-fluorophenylboronic acid, respectively, in the presence of a palladium catalyst. The chemical structures and compositions of the resulting precursor and spiro-compounds were characterized

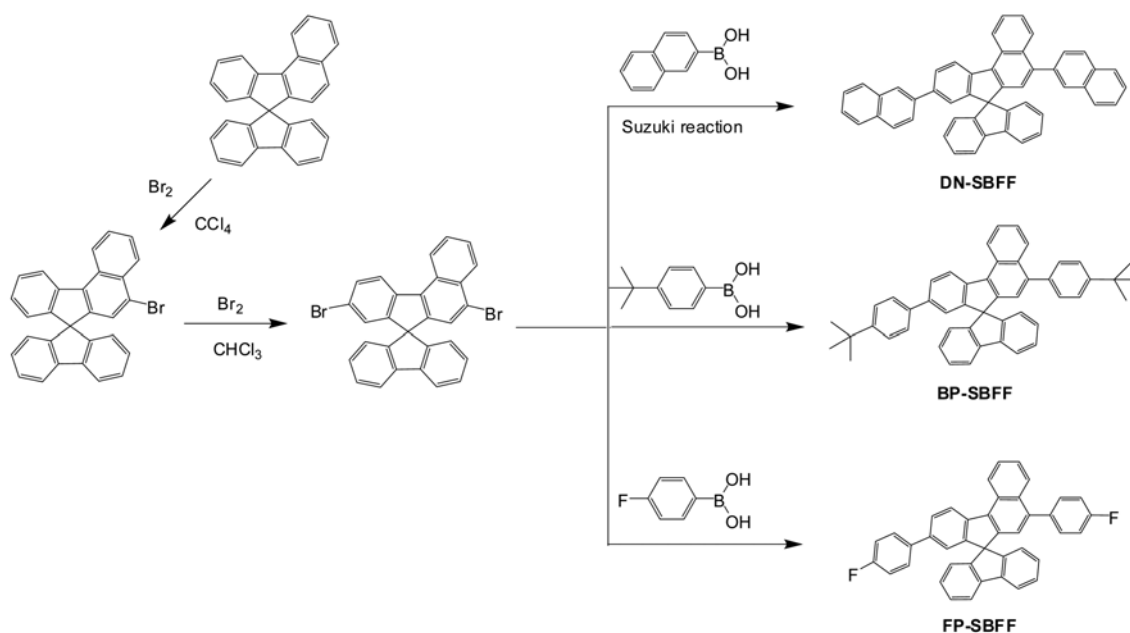
by <sup>1</sup>H NMR, <sup>13</sup>C NMR, FT-IR, GC-MS, and by elemental analysis.

**Thermal Properties.** The thermal properties of the resulting blue host materials were characterized by DSC and TGA in a nitrogen atmosphere. Their decomposition temperatures (at onset) were 461, 436, and 375 °C for **DN-SBFF**, **BP-SBFF**, and **FP-SBFF**, respectively, as summarized in Table 1. **DN-SBFF** had a melting point (*T*<sub>m</sub>) of 246.5, but on second heating no melting point was observed for any of the three hosts, despite being allowed to cool in air. In fact, after they achieved the amorphous state, they did not revert to the crystalline state. After the samples had cooled to room temperature, a second DSC scan was performed at 10 °C/min, and revealed high glass transition temperatures (*T*<sub>g</sub>) of 201, 166 and 198 °C for **DN-SBFF**, **BP-SBFF** and **FP-SBFF**, respectively. This suggests that the thermal stability of all three was significantly improved by the introduction of the rigid aromatic unit into the spiro-type backbone. The amorphous states of transparent films of the three host materials showed that they were good candidates for use as EL materials.

**Optical Properties and Energy Levels.** Table 1 and Figure 2 show the absorption and photoluminescence (PL) spectral data and other optical properties of the host materials. The solution absorption maxima of **DN-SBFF**, **BP-SBFF**, and **FP-SBFF** were at 364, 359 and 355 nm, respectively, and the emission maxima of all three in solu-



**Scheme 2.** Schematic routes to dopant material **TPA-SBFF**.



**Scheme 3.** Schematic routes to synthesize spiro[benzo[*c*]fluorene-7,9'-fluorene] derivatives.

**Table 1.** UV absorption, PL, energy levels and thermal properties of three host materials

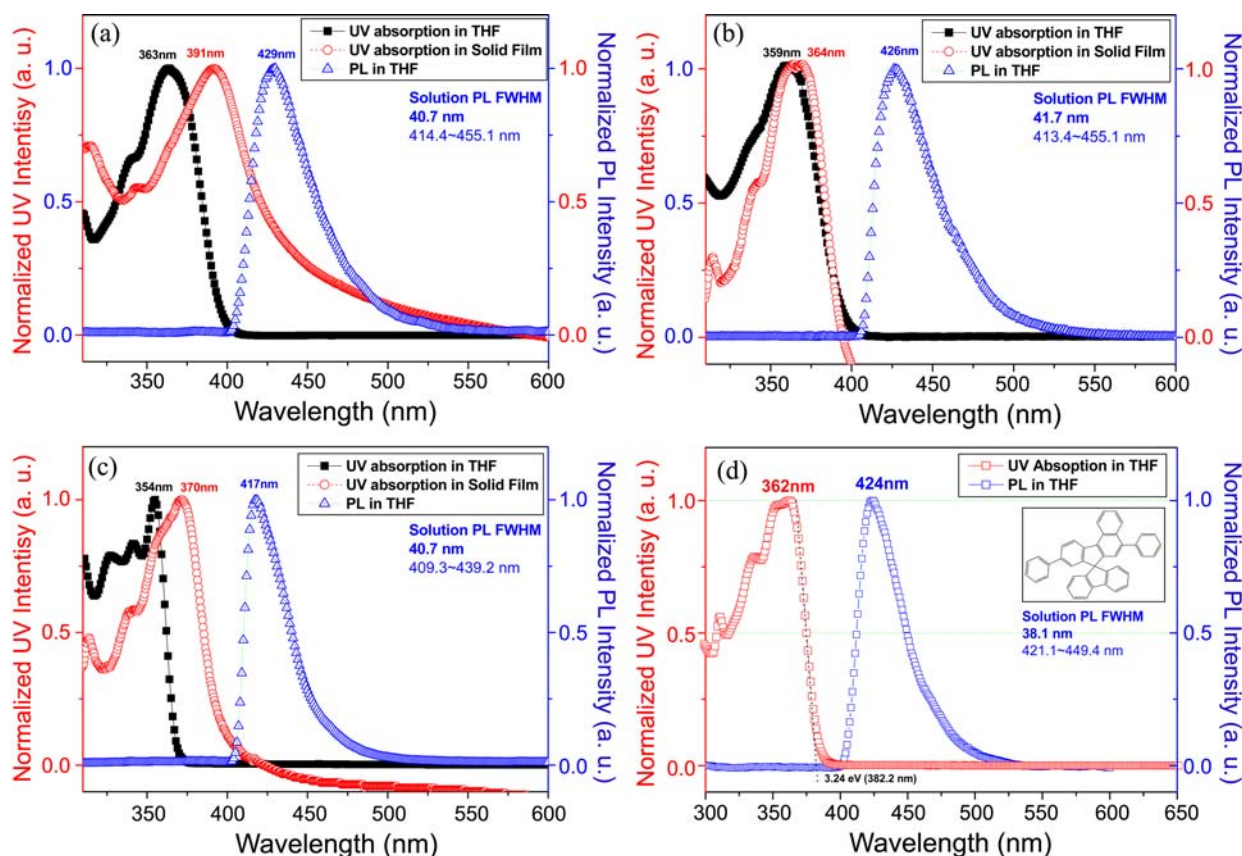
Properties		Samples <sup>a</sup>		
		DN-SBFF	BP-SBFF	FP-SBFF
Thermal analysis	T <sub>m</sub> (°C)	256.5	259	259
	T <sub>d</sub> (°C)	462	436	375
	T <sub>g</sub> (°C)	201	166.1	198.9
UV	Max (nm)	364	359	355
	Bg <sup>b</sup> (eV)	3.13	3.14	3.36
Solid UV	Max (nm)	369	391	371
	PL			
Optical analysis	Max (nm)	430	426	418
	FWHM <sup>c</sup> (nm)	40.7	41.7	40.7
Solid PL	Max (nm)	424.8	418	418.4
	QE			
Electrical analysis	Φ <sub>r</sub> <sup>d</sup>	0.61	0.66	0.58
	HOMO (eV)	5.44	5.92	5.97
	LUMO (eV)	2.31	2.78	2.61

<sup>a</sup>The purity of the samples were finally determined as >99.9% by high performance liquid chromatography (HPLC) using the above prepared samples after train sublimation. <sup>b</sup>Bandgap. <sup>c</sup>Full width at half maximum. <sup>d</sup>Fluorescence quantum efficiency, relative to 9,10-diphenylanthracene in cyclohexane (Φ<sub>r</sub> = 0.90).

tion lay between 418 and 430 nm. Furthermore, in solution, they still showed a deep blue emission peak without significant shift in the PL spectrum, despite the introduction of aromatic moieties at the 5- and 9-positions in SBFF core. Comparing with the reference compound, 5,9-diphenyl-

SBFF, which has an Abs<sub>max</sub> at 362 nm and a blue PL<sub>max</sub> at ~424 nm, the three host materials did not show any apparent change in absorption or emission spectra, as shown in Figure 2(d). Interestingly, BP-SBFF and FP-SBFF possessed electron donating and attracting groups. The solution fluorescence quantum efficiencies (Φ<sub>r</sub>) of the host materials ranged from 0.58 to 0.66 relatively small than that of 9,10-diphenylanthracene in cyclohexane (Φ<sub>r</sub> = 0.90). The relatively higher fluorescence quantum efficiency value of BP-SBFF as compared with BH-6SFP was attributed to the introduction of the *tert*-butyl groups, which prevent intermolecular interaction between the BP-SBFF molecules.

Molecular simulations of DN-SBFF, BP-SBFF, and FP-SBFF were carried out in an attempt to understand their physical properties at the molecular level. Density functional theory (DFT) calculations have been previously performed to characterize the three-dimensional geometries and the frontier molecular orbital energy levels of three host materials at the B3LYP/6-31G\* level using the Gaussian 03 program.<sup>20</sup> The electron densities in HOMOs were mostly localized on the benzofluorene unit with some orbital distribution in the side phenyl rings. The LUMO distributions of the hosts were similar to their HOMO distributions, indicating their HOMO and LUMO levels are dominated by the benzofluorene core structure and that the aromatic moieties at the 5- and 9-positions slightly affect their HOMO and LUMO orbital distributions. The aromatic moieties may cause a shift in the HOMO and LUMO levels of the benzo-

**Figure 2.** UV-vis and PL spectra of (a) DN-SBFF, (b) BP-SBFF, (c) FP-SBFF, and (d) 5,9-diphenyl-SBFF.

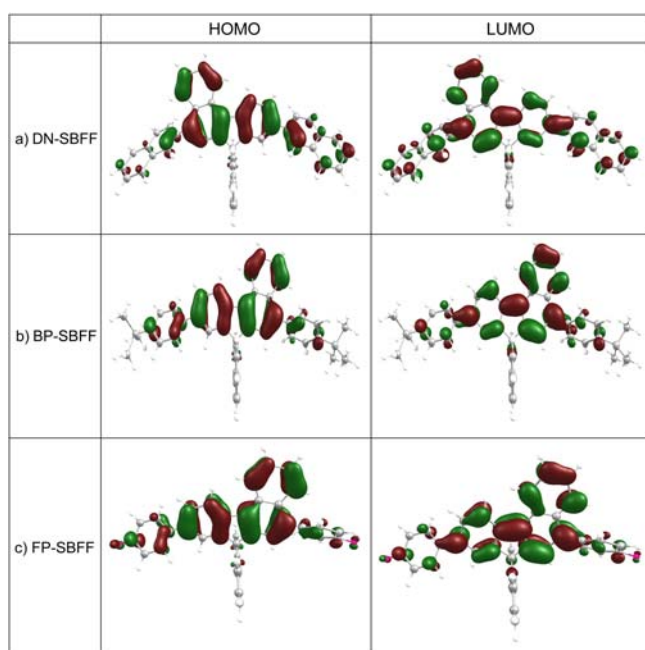


**Figure 3.** Molecular orbital distribution of the (a) DN-SBFF, (b) BP-SBFF, and (c) FP-SBFF.

fluorene group, which suggests that the absorption and emission processes are attributable to  $\pi$ - $\pi^*$  transition centered at the benzofluorene unit. Accordingly, the molecular orbital analyses indicated that the fluoro and *t*-butyl moieties of the aromatic rings in spirofluorene did not affect the HOMO and LUMO distributions of the host materials. These geometrical characteristics can effectively prevent intermolecular interactions between  $\pi$ -systems, and thus, suppress molecular crystallization, which would improve the morphological stabilities of these molecules.

The energy levels of three host and dopant materials used to fabricate OLEDs in the present study are shown in Figure 4. A low-energy photoelectron spectrometer was used to obtain information on the HOMO energies of the host and dopant materials and to examine charge injection barriers. Energy gaps for DN-SBFF, BP-SBFF, and FP-SBFF were calculated to be 3.13 eV, 3.14 eV, and 3.36 eV, respectively, which corresponded to the absorption wavelengths of 396, 395 and 369 nm, respectively. The HOMO energy levels of host and dopant materials were determined to be 5.44, 5.92, 5.97, and 5.48 eV for DN-SBFF, BP-SBFF, FP-SBFF and TPA-SBFF, respectively. The HOMO value of DN-SBFF was lower than that of the other two hosts because of its expanded conjugation length.

**EL Properties.** In order to determine optimum dopant concentrations, the EL spectra of DN-SBFF, BP-SBFF, and

**Table 2.** EL properties of the devices obtained from three hosts and TPA-SBFF dopant

Properties	Devices			
	DN-SBFF	BP-SBFF	FP-SBFF	
$\lambda_{\max}$ (nm)	466	460	463	
FWHM (nm)	57	51	54	
mA/cm <sup>2</sup>	3.12	3.75	4.69	
cd/A <sup>a</sup>	7.14	3.38	6.61	
cd/A <sup>b</sup>	7.14(7 V)	4.10(5 V)	6.61(7 V)	
EL at 7 V	cd/A <sup>c</sup>	1.67	1.01	1.21
lm/W	3.35	1.51	3.26	
cd/m <sup>2</sup>	141	55.5	183.6	
CIE-x	0.140	0.140	0.140	
CIE-y	0.169	0.166	0.172	
EQE (%)	4.69	2.53	4.31	

<sup>a</sup>Values at 7 V. <sup>b</sup>values at a highest peak. <sup>c</sup>Values obtained without dopant.

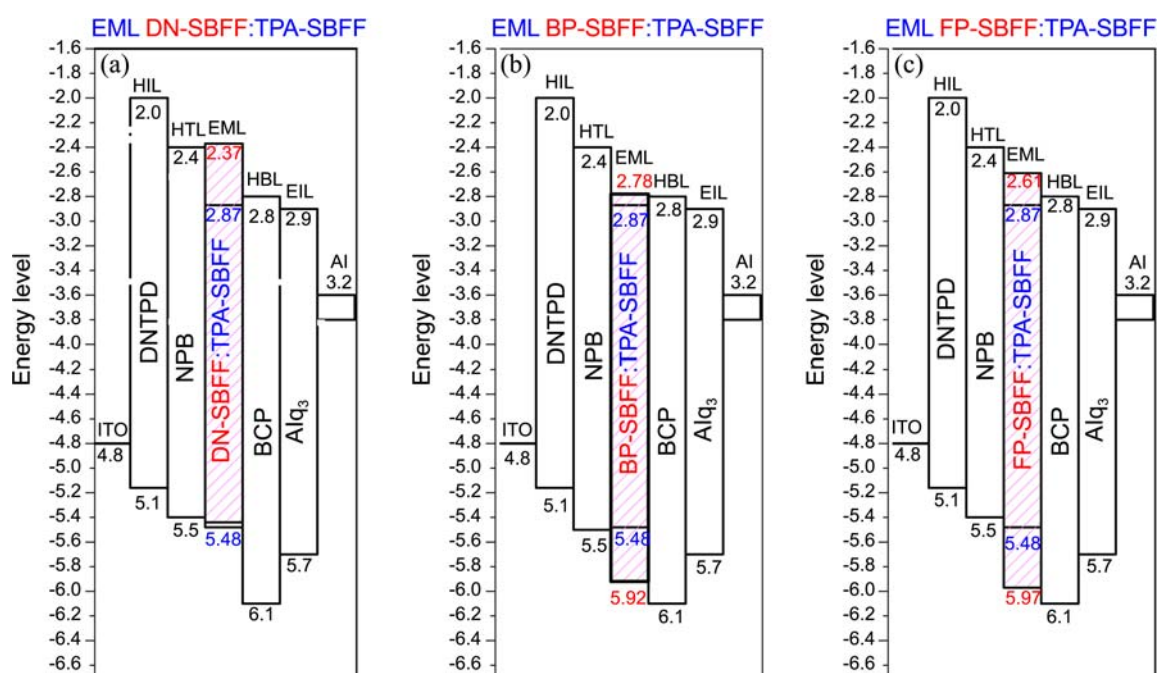


**Figure 4.** Energy diagrams of (a) DN-SBFF, (b) BP-SBFF and (c) of FP-SBFF doped with TPA-SBFF.

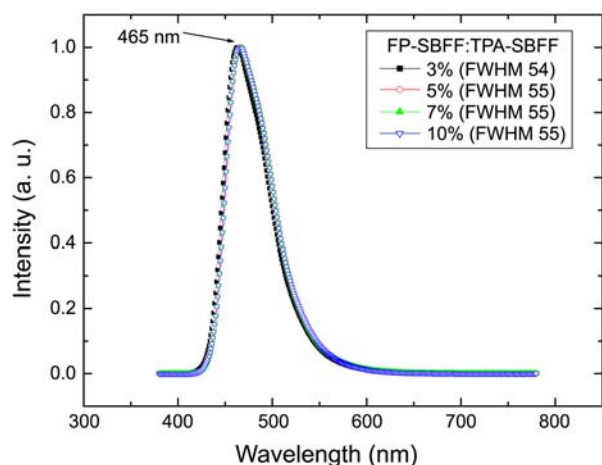


**Figure 5.** EL spectra of the FP-SBFF devices doped with TPA-SBFF.

FP-SBFF doped by TPA-SBFF at different concentrations (3%, 5%, 7% and 10%) were obtained. The EL spectra of blue fluorescent FP-SBFF devices doped with TPA-SBFF showed a maximum peak at 465 nm as shown in Figure 5. Pure deep blue emission was observed from the TPA-SBFF-doped device showing color coordinates ( $x = 0.138$ - $0.141$ , and  $y = 0.144$ - $0.202$ ). The EL spectra of other hosts were similar to that of FP-SBFF (Table 2). The peak maximum of EL spectra at 465 nm was consistent even at high doping concentrations. EL emission obtained from the host was dominated by the PL peak of the host, which suggests that energy transfer from the host to dopant is efficient at the optimum dopant concentration employed in this experiment. The full width at half maximum (FWHM, 55 nm) of EL peak was relatively small, which leads to good color purity as illustrated in the PL (FWHM, 40 nm) spectrum. The dependence of chromaticity on the current density was measured to evaluate the stability of the devices (Figure 6). When the EL spectrum was converted into chromaticity coordinates on the CIE 1931 diagram, the chromaticity was found to decrease with dopant concentration. Furthermore, the stability of CIEx coordinate was better than that of CIEy

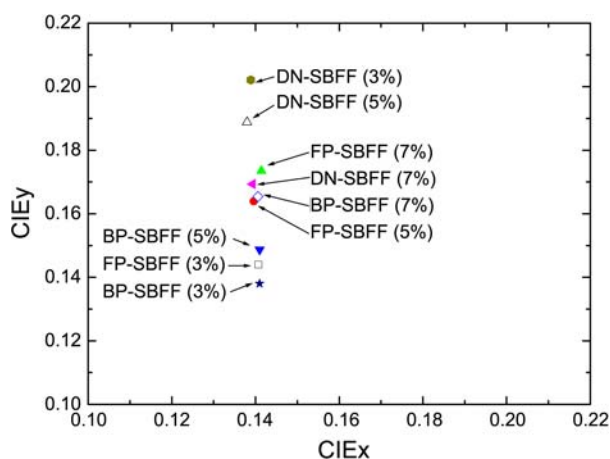


**Figure 6.** CIE 1931 coordinate of the devices obtained from the three host materials.

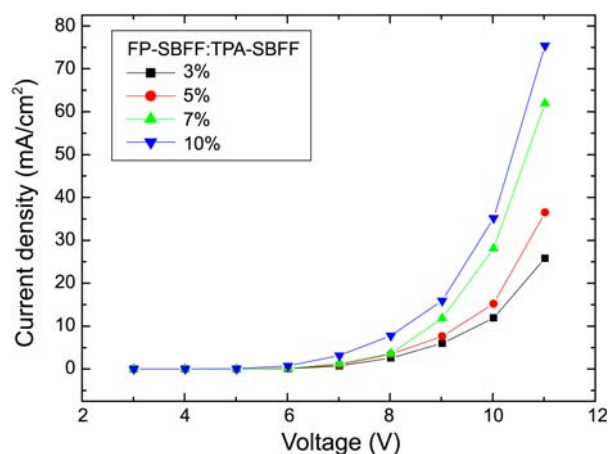


**Figure 7.** Current density-voltage characteristics of the FP-SBFF devices doped with 3, 5, 7 or 10% TPA-SBFF.

coordinate. The FP-SBFF device (3% dopant) emitted a deep blue light with CIE coordinates of (0.140, 0.144).

**OLED Device Properties.** Figures 7 and 8 shows the luminance-voltage and current density-voltage characteristics of the OLEDs with FP-SBFF doped with 3%, 5%, 7%, and 10% TPA-SBFF dopant, respectively, as the emitting layer. When 7% of TPA-SBFF was used, the highest luminance efficiency and the best color purity were observed for DN-SBFF. Increasing the doping concentration to 10% reduced luminance efficiency presumably because of the concentration quenching effect. The threshold voltage for luminescence was about 5.0 V for all devices. In the case of the DN-SBFF device doped with 3% TPA-SBFF, the maximum brightness ( $141 \text{ cdm}^{-2}$ ) was obtained at approximately 7.0 V (Table 2). The DN-SBFF device doped with 7% TPA-SBFF showed higher current density and luminance than the FP-SBFF device doped with 7% TPA-SBFF at the same driving voltage. Decreases in the current density and luminance of the DN-SBFF device were attributed to the wide bandgap of DN-SBFF. The luminance efficiency of DN-SBFF device doped with 7% dopant was 5 times higher than that of the device without dopant, which suggests that

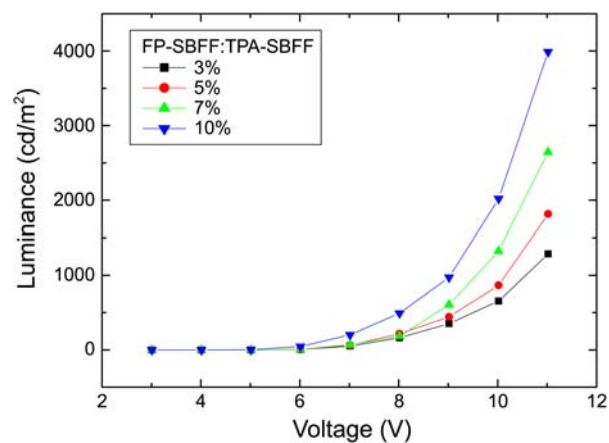


**Figure 8.** Luminance-voltage characteristics of the FP-SBFF devices doped with 3, 5, 7 or 10% TPA-SBFF.

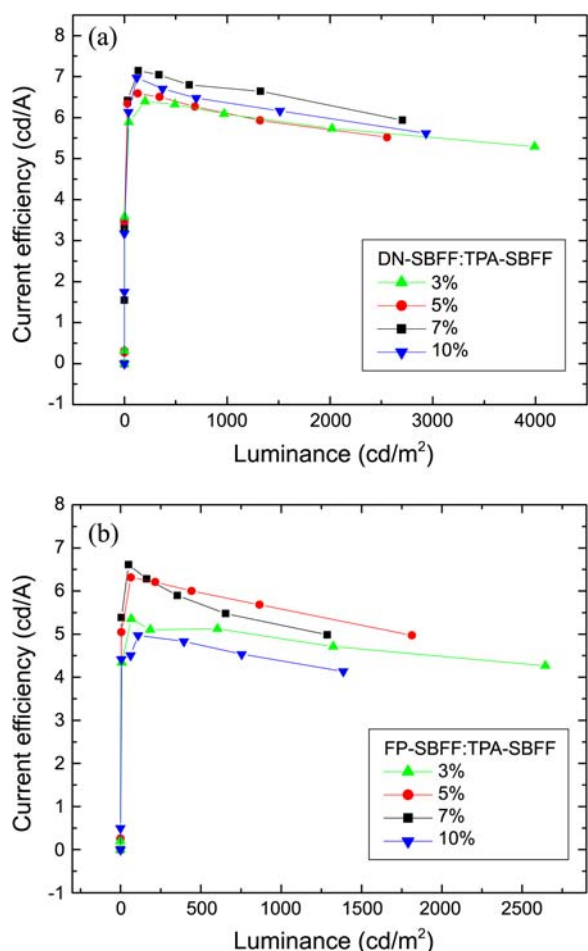


**Figure 9.** Current efficiency-luminance characteristics of the devices obtained from (a) DN-SBFF and (b) FP-SBFF doped with 3, 5, 7 and 10% TPA-SBFF.

dopant substantially enhances the EL properties of spiro-type emitting layers.

Figure 9 shows relation between luminance efficiency and current density for four devices. The maximum power efficiency of the DN-SBFF device doped with 7% TPA-SBFF was 3.35 lmW<sup>-1</sup>. This device had a maximum EQE of 4.69% and its efficiency increased rapidly to 7.14 cdA<sup>-1</sup> at a low current density of 3.12 mAcm<sup>-2</sup> at 7 V. The holes injected from a hole transfer layer,  $\alpha$ -NPB, were transferred to the emitting layer and can be trapped to dopant sites. HOMO values of the three dopant materials increased in the order of DN-SBFF (5.44 eV) < BP-SBFF (5.92 eV) < FP-SBFF (5.97 eV). Because the HOMO values of TPA-SBFF (5.48 eV) and DN-SBFF were similar to each other, the holes from  $\alpha$ -NPB were easily transferred to ETL and emission layer. However, TPA-SBFF had a capacity to catch holes strongly and to minimize hole loss, which resulted in good electroluminescent efficiency. Thus, the HOMO level of TPA-SBFF was found to be suitable for hole trapping and the hole transport as a dopant. On the other hand, the DN-SBFF host was found to be appropriate for balancing the number of holes and electrons in the emitting layer.

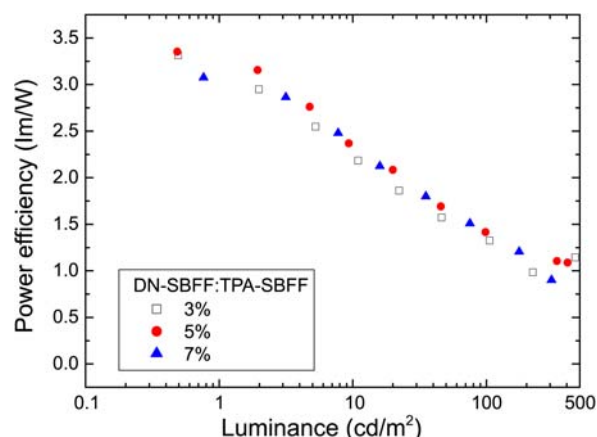


**Figure 10.** Power efficiency-luminance curves of the DN-SBFF devices doped with various dopant concentration.

At low doping concentrations, electron transfer occurred mainly by the host, and electron transfer of DN-SBFF seemed to be faster than that of FP-SBFF. Actually, the high conjugation usually assisted electron injection and movement but did not improve hole movement, whereas electron-deficient FP-SBFF was incapable of accepting an electron around its benzofluorene unit.<sup>18,21,22</sup> The HOMO of FP-SBFF was delocalized in the fluorophenyl unit, which decreased its electron transporting ability. In addition, it was found FP-SBFF doped with 7% TPA-SBFF had a relatively high efficiency and that this decreased only slightly when as the current density was increased to 4.69 mAcm<sup>-2</sup>. In fact, it reached a current efficiency of 6.61 cdA<sup>-1</sup>. This suggests that an exciton is formed and light is emitted at specific thresholds. It should be noted that the efficiencies of these devices did not decrease significantly when the current density was increased to 4.69 mAcm<sup>-2</sup>. The BP-SBFF device doped with 7% TPA-SBFF had a maximum EQE of 2.53% at a current density of 3.75 mAcm<sup>-2</sup> (5 V, 55.5 cdm<sup>-2</sup>) and an luminance efficiency of 4.10 cdA<sup>-1</sup>, a power efficiency of 2.51 lmW<sup>-1</sup>, and CIE coordinates of (0.140, 0.150).

The power efficiencies of the DN-SBFF devices with various dopant concentrations are shown in Figure 10. The

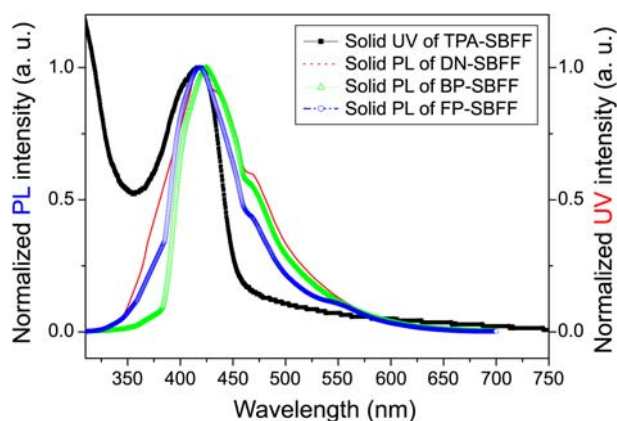


**Figure 11.** UV-vis absorption spectrum of TPA-SBFF and PL spectra of three host materials, DN-SBFF, BP-SBFF, and FP-SBFF.

maximum power efficiency of the **DN-SBFF** devices was similar, but decrease in power efficiency at high luminance was significant. This decrease in power efficiency at high luminance was attributed to the high-energy barrier of hole injection in the **DN-SBFF** device. Although holes and electrons are balanced at low luminance, more electron injection at high driving voltages disrupts the hole/electron balance in the emitting layer because of limited hole injection, which leads to low power efficiency at high luminance.

The PL spectrum of three hosts showed considerable overlap in the absorption spectrum of **TPA-SBFF** as shown in Figure 11. This indicates that **TPA-SBFF** can effectively accept energy from the host by Förster energy transfer or function as a direct recombination center due to its higher HOMO levels.<sup>21,23</sup> By using **FP-SBFF** as host and **DB-6DPA** fluorescent dopant, the PE was successfully enhanced to  $3.26 \text{ lmW}^{-1}$ , which is four times higher than that of the undoped device. The EQE of OLEDs using **TPA-SBFF** as fluorescent dopant at a concentration of 7 wt % was 4.41% with CIE coordinates of (0.141, 0.172).

### Conclusion

New fluorescence blue host materials based on spiro[benzo[*c*]fluorene-7,9'-fluorene] derivatives were successfully prepared and used to construct blue OLEDs. The EL emission spectra of 465 nm. The CIE coordinates of the **FP-SBFF** device doped with 7% **TPA-SBFF** the devices were around was (0.140, 0.166), which are suitable color coordinate values for blue emission. The **DN-SBFF** device doped with 7% **TPA-SBFF** had a maximum luminance of  $141 \text{ cd/m}^2$  at a current density of  $3.12 \text{ mA/cm}^2$ , and a maximum power efficiency of  $7.14 \text{ cd/A}$ . According to these characteristics, these deep-blue emitting materials have sufficient potential for use in fluorescence OLED applications.

### References

1. Tang, C. W.; Van Slyke, S. A.; Chen, C. H. *J. Appl. Phys.* **1989**, 65, 3610.
2. Adachi, C.; Tsutsui, T.; Saito, S. *Appl. Phys. Lett.* **1989**, 55, 1489.
3. Baldo, M. A.; Thompson, M. E.; Forrest, S. R. *Nature* **2000**, 403, 750.
4. Wu, C. C.; Lin, Y. T.; Wong, K. T.; Chen, R. T.; Chien, Y. Y. *Adv. Mater.* **2004**, 16, 61.
5. Im, W. B.; Hwang, H. K.; Lee, J. G.; Han, K.; Kim, Y. *Appl. Phys. Lett.* **2001**, 79, 1387.
6. Kijima, Y.; Asai, N.; Tamura, S. I. *Jpn. J. Appl. Phys. Part 1* **1999**, 38, 5227.
7. Wu, Z.; Zheng, X. Y.; Zheng, W. Q.; Zhu, W. Q.; Sun, R. G.; Jiang, X. Y.; Zhang, Z. L.; Xu, S. H. *Appl. Phys. Lett.* **2003**, 83, 5077.
8. Xiong, Y.; Xu, W.; Li, C.; Liang, B.; Zhao, L.; Peng, J.; Cao, Y.; Wang, J. *Org. Electron.* **2008**, 9, 533.
9. Jeon, S. O.; Jeon, Y. M.; Kim, J. W.; Lee, C. W.; Gong, M. S. *Org. Electron.* **2008**, 9, 522.
10. Jeon, S. O.; Jeon, Y. M.; Kim, J. W.; Lee, C. W.; Gong, M. S. *Synth. Met.* **2009**, 159, 1147.
11. Hamai, S.; Hirayama, F. *J. Phys. Chem.* **1983**, 87, 83.
12. Kim, K. S.; Lee, H. S.; Jeon, Y. M.; Kim, J. W.; Lee, C. W.; Gong, M. S. *Dyes Pigm.* **2009**, 81, 174.
13. Jeon, Y. M.; Kim, J. W.; Lee, C. W.; Gong, M. S. *Dyes Pigm.* **2009**, 83, 66.
14. Kim, K. S.; Lee, H. S.; Jeon, Y. M.; Kim, J. W.; Lee, C. W.; Gong, M. S. *Synth. Met.* **2008**, 158, 870.
15. Kim, K. S.; Jeon, Y. M.; Kim, J. W.; Lee, C. W.; Gong, M. S. *Org. Electron.* **2008**, 9, 797.
16. Kim, J. H.; Jeon, Y. M.; Jang, J. G.; Ryu, S.; Chang, H. J.; Lee, C. W.; Kim, J. W.; Gong, M. S. *Bull. Korean Chem. Soc.* **2009**, 30, 647.
17. Jeon, S. O.; Lee, H. S.; Jeon, Y. M.; Kim, J. W.; Lee, C. W.; Gong, M. S. *Bull. Korean Chem. Soc.* **2009**, 30, 863.
18. Jeon, Y. M.; Lee, J. Y.; Kim, J. W.; Lee, C. W.; Gong, M. S. *Org. Electron.* **2011**, 11, 1844.
19. Lee, I. H.; Gong, M. S. *Bull. Korean Chem. Soc.* **2011**, 32, 1475.
20. Frisch, M. J. *et al.*, *GAUSSIAN 03*, Revision B.05, Gaussian, Inc., Pittsburgh, PA, 2003.
21. Lee, S. J.; Park, J. S.; Yoon, K. J.; Kim, Y. I.; Jin, S. H.; Kang, S. K.; Gal, Y.; Kang, S.; Lee, J. Y.; Kang, J.; Lee, S. H.; Park, H. D.; Kim, J. J. *Adv. Funct. Mater.* **2008**, 18, 3922.
22. Jeon, Y. M.; Lee, I. H.; Lee, C. W.; Lee, J. Y.; Gong, M. S. *Bull. Korean Chem. Soc.* **2010**, 31, 2955.
23. Jeon, Y. M.; Lee, H. S.; Gong, M. S. *J. Mater. Chem.* **2010**, 20, 10735.